NANO LETTERS

LETTER

pubs.acs.org/NanoLett

Surface Enhanced Coherent Anti-Stokes Raman Scattering on Nanostructured Gold Surfaces

Christian Steuwe,[†] Clemens F. Kaminski,[‡] Jeremy J. Baumberg,*[,†] and Sumeet Mahajan*[,†]

[†]Cavendish Laboratory, University of Cambridge, J. J. Thomson Avenue, Cambridge, CB3 0HE, United Kingdom

[‡]Dept. of Chemical Engineering and Biotechnology, University of Cambridge, Pembroke Street, CB2 3RA, United Kingdom

Supporting Information

ABSTRACT:

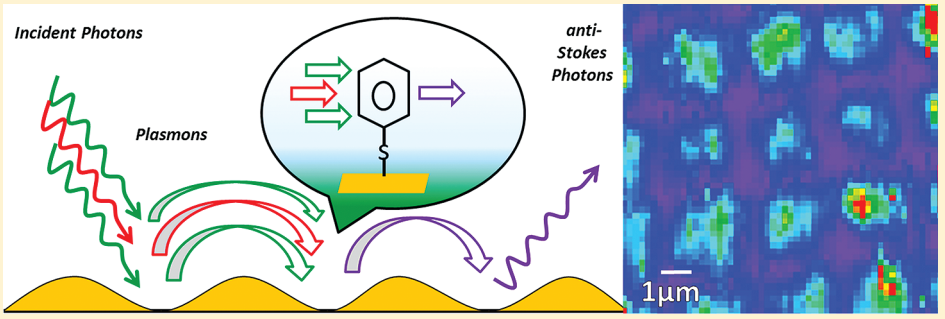

Coherent anti-Stokes Raman spectroscopy (CARS) is a well-known tool in multiphoton imaging and nonlinear spectroscopy. In this work we combine CARS with plasmonic surface enhancement on reproducible nanostructured surfaces. We demonstrate strong correlation between plasmon resonances and surface-enhanced CARS (SECARS) intensities on our nanostructured surfaces and show that an enhancement of $\sim 10^5$ can be obtained over standard CARS. Furthermore, we find SECARS to be $>10^3$ times more sensitive than surface-enhanced Raman Spectroscopy (SERS). We also demonstrate SECARS imaging of molecular monolayers. Our work paves the way for reliable single molecule Raman spectroscopy and fast molecular imaging on plasmonic surfaces.

KEYWORDS: Plasmons, surface-enhancement, coherent anti-Stokes Raman, nanostructures, SECARS

Raman scattering is a widely used method to identify molecules by means of their vibrational fingerprint. However, spontaneous Raman is incredibly weak with a cross-section[1] of $\sim 10^{-30}$ cm^2 and therefore various techniques have been applied to increase its sensitivity. Coherent anti-Stokes Raman scattering[2] (CARS) utilizes a nonlinear four-wave mixing process resulting in much higher sensitivity than spontaneous Raman and has been employed in vibrational bioimaging since the late nineties.[3] CARS is a third order nonlinear effect where three photons ω_1, ω_2, and ω_3 of two different frequencies ω_s and ω_p interact coherently through the third-order susceptibility ($\chi^{(3)}$) of the material producing a spectrally separated, blue-shifted photon at the anti-Stokes frequency ω_{as} (Figure 1). Although CARS is more sensitive than conventional Raman due to its higher order dependence on incident power, its sensitivity is still not enough for monitoring or imaging molecules present in extremely low concentrations. Moreover reduced photodamage and faster real-time acquisition is highly desirable in bioimaging applications and hence it is crucial to achieve higher sensitivities. One way to achieve higher sensitivities is to employ surface plasmons generated on nanostructures to enhance CARS signals. This is illustrated schematically in Figure 1, which shows the transitions and field dependence of signals in various Raman processes. Although plasmonic enhancement of Raman scattering

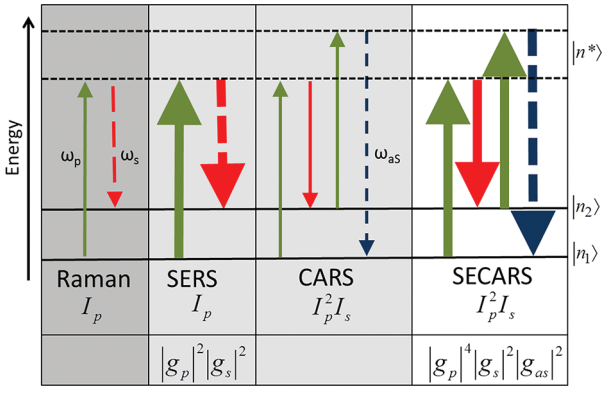

Figure 1. Schematic band energy diagram showing transitions in different Raman processes and their dependence on the pump and Stokes intensity (I_{pump} and I_{Stokes}) and local electric field enhancement (g). The Dirac notation $|n^*\rangle$ denotes virtual states of the molecules while $|n_1\rangle$ and $|n_2\rangle$ symbolize its vibrational ground and first excited state.

Received: August 19, 2011
Revised: November 4, 2011

   dx.doi.org/10.1021/nl202875w | *Nano Lett.* XXXX, XXX, 000–000

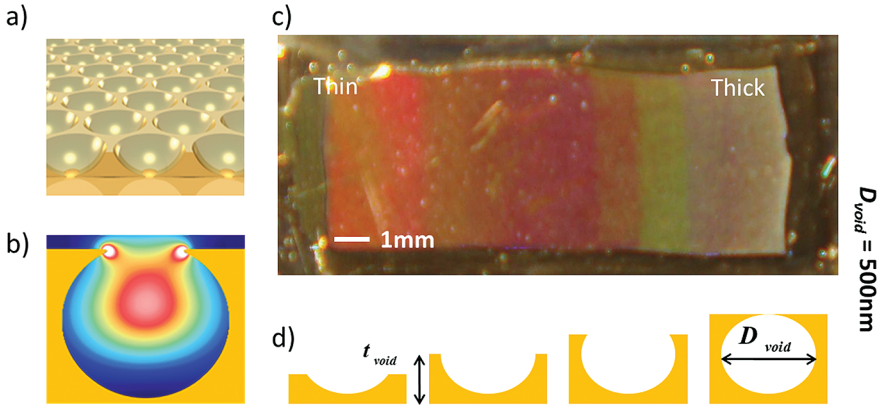

Figure 2. (a) Schematic of a nanovoid gold surface. (b) Example of electric field distribution inside a nanovoid for one plasmon mode simulated using the boundary element method.[23] Strong field enhancement occurs at the rim of the nanovoid in this case. (c) A photograph of a graded nanovoid surface. The samples' varying thickness t_{void} is clearly distinguishable by varying colors due to the shifting plasmonic absorption modes. A single sample consists of graded structures from shallow dishes to almost encapsulated spherical voids, schematically shown below the photograph in (d). This variation is represented by a normalized thickness $\bar{t} = t_{void}/D_{void}$.

(SERS[4−6]) and fluorescence on surfaces[7] has been widely studied over the last three decades, only a few such attempts have been made with CARS. A few studies with colloidal silver and gold nanoparticles exist;[8−12] furthermore, Hayazawa et al. reported the enhancement using modified AFM tips in CARS (called tip-enhanced CARS).[13,14] No work has yet been reported on the combination of CARS with reproducible plasmonic surfaces. In the colloidal studies, the enhancement is due to "hot-spots" of highly localized electric fields at the nanoparticle junctions and a 10−100 times signal enhancement over conventional CARS is usually observed. Although theoretically higher enhancements, up to 10^{12}, are predicted,[15] they have not been reproduced in experiments. The CARS signal will be enhanced if any of the photons ω_s, ω_p, or ω_{as} is in resonance with the supported plasmons although the local fields at the three different frequencies may contribute individually. For the strongest enhancements, all three photons should be in resonance with the nanoparticle in same spatial location.[15] However, with metal nanospheres this is unlikely[16] and hence only weak CARS plasmonic enhancements of molecules in the proximity of nanoparticles are observed.

In this work, we use nanovoid surfaces that show large reproducible enhancements in surface-enhanced Raman spectroscopy[17,18] (SERS). In contrast to nanospheres, void surfaces show broad plasmon absorptions over a large spectral range that can be comprehensively tuned through appropriate design of nanoarchitectures.[19] Hence pump, Stokes, and anti-Stokes photons can simultaneously be in resonance with the substrate, which is impossible for nanoparticles. Furthermore, the resonances are easily tuned by varying the void size and the thickness of films in these plasmonic surfaces to match any suitable lasers.[20] Using nanovoid samples here we demonstrate the resonant plasmon dependence of SECARS signals. We find that strong additional enhancements of ~10^5 occur over CARS when pump, Stokes, and anti-Stokes frequencies coincide with plasmon resonances. We also demonstrate the molecular specificity of the SECARS signals and verify its power dependence. Furthermore, by careful calibration we find that SECARS intensities are enhanced by ~10^3 over SERS. This gives an overall enhancement of 10^9−10^{10} for SECARS over spontaneous Raman. Using benzenethiol as a Raman marker we are also able to image a monolayer on a commercially available plasmonic substrate, Klarite, which also has well-defined broad resonances[21] using SECARS. Thus, our study paves the way for straightforward and reproducible ultrasensitive molecular monitoring and imaging on plasmonic surfaces.

For SECARS, our nanostructured plasmonic surfaces are excited by two incident laser beams of frequencies ω_p and ω_s. The third-order CARS susceptibility gives rise to a nonlinear polarization at $\omega_{CARS} = 2\omega_p - \omega_s$ allowing for detection of a signal that is blue-shifted from the incident laser beams. The high intensity of SECARS signals permits both laser beams to be generated by a single 80 MHz pulsed Ti:Sapphire oscillator with an average power of 1.4 W at 800 nm, greatly simplifying the setup and reducing costs over multilaser CARS configurations. This laser beam is split into two branches: one branch forms the pump beam at ω_p while the other is used to generate a supercontinuum between 830 and 1100 nm through a photonic crystal fiber. The spatially and temporally overlapped beams are fed into a microscope and detection is carried out in the back-reflection mode (in Epi configuration). Typically, experiments were performed with a laser power of 30 mW in the pump and 1.1 mW in the Stokes per contributing line corresponding to an average power density of 3.9×10^6 W cm^{-2} (and a peak power density of 3×10^{11} W cm^{-2}) within a diffraction limited spot of 1μm diameter (Rayleigh limit; = 0.61 λ/N_A). The average power densities are similar to those used in typical SERS experiments. The blue-shifted light at ω_{CARS} is detected by a spectrometer. This "Broadband CARS" setup (see Supporting Information, Section 1.1 for details) is capable of taking a full CARS spectrum (over ~2000 cm^{-1}) within a single integration (1−100 ms). The setup is stable over time spans of hours with only minor fluctuations in the Stokes spectrum.

Our nanovoid surfaces are fabricated with a nanotemplating process using colloidal polystyrene beads that are self-assembled on a gold-coated glass slide producing monolayers of well-ordered close-packed spheres. Templates with sphere diameters, D, between 100 nm and several micrometers are easily achieved using this method.[22] Electrodeposition is carried out through these templates and the charge passed allows accurate control of the metal thickness, t_{void}. By systematically retracting the sample from the plating bath during growth, the nanostructure geometry is graded (Figure 2c,d) producing different thicknesses across the

dx.doi.org/10.1021/nl202875w |Nano Lett. XXXX, XXX, 000–000

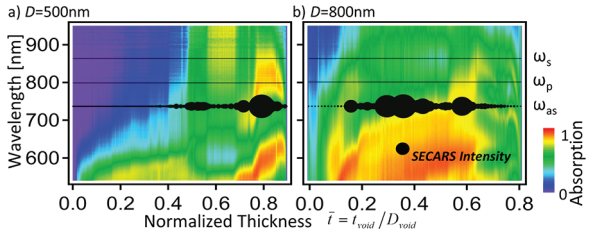

Figure 3. Correlation of plasmon absorption with SECARS. Position-resolved extinction maps of nanovoid surfaces fabricated with (a) 500 nm and (b) 800 nm diameter sphere templates. Areas displayed in red indicate maximum extinction and purple areas show the least. The SECARS signal is overlaid on the extinction map (at the anti-Stokes wavelength of 736 nm) with the size of circles proportional to the normalized intensity of the 1070 cm^{-1} peak. Solid black lines are for the Stokes and pump wavelength at 875 nm and 800 nm, respectively. Note that the contribution of plasmons excited at the pump wavelength of 800 nm is higher than that of either Stokes and anti-Stokes plasmons, due to the two pump plasmons involved in the SECARS process.

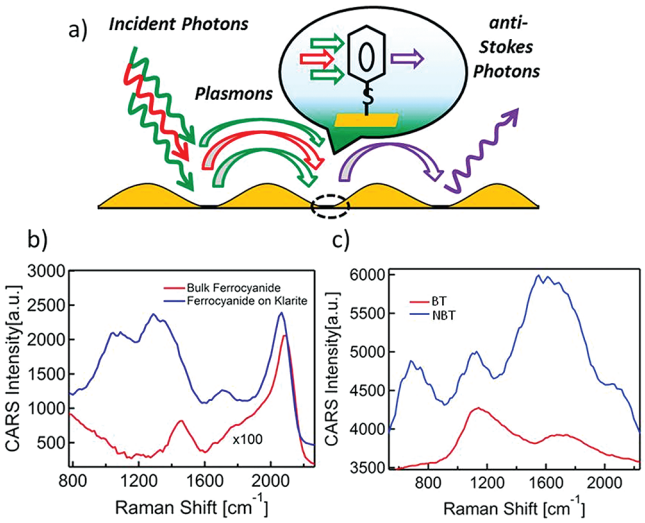

Figure 4. (a) Model for surface-enhanced CARS. Incoming pump and Stokes radiation couples into respective plasmons that interact coherently with a molecule on the surface. The outgoing CARS scattered plasmon is coupled into an emitted anti-Stokes photon. (b) SECARS spectrum (blue) of submonolayer cyanide salt on Klarite showing expected peak at 2150 cm^{-1}, as also observed in CARS (red) of the same bulk cyanide salt. (c) SECARS spectra of nitrilobenzenethiol (NBT) and benzenethiol (BT) on Klarite.

same sample. After deposition the template is dissolved, leaving the nanovoid structure in Figure 2a. Thus shallow dishes as well as almost encapsulated spherical voids are created on a single sample. Nanovoid surfaces give strong field enhancements with well-characterized localized Mie and delocalized Bragg plasmons[19,23] that vary systematically with their geometry. One such plasmon mode with its electric field distribution is shown in Figure 2b. Given the tunability of plasmonic properties with nanovoid geometry,[24,25] these surfaces are ideal to study the plasmon dependence of SECARS.

To demonstrate the plasmon resonance dependence of SECARS, extinction spectra for all graded samples with void diameters between 400 and 1000 nm are taken. For mapping the plasmon absorption, samples were mounted on an $X-Y$ translation stage and scanned along the graded direction (direction of variation in thickness) of the nanovoid sample with an extinction spectrum taken every 150 μm.

Figure 3 shows the extinction map of a graded 500 nm sphere diameter Au nanovoid substrate that reveals several distinct plasmon modes tuning rapidly with geometry as discussed in detail elsewhere.[19,23] A strong extinction around the pump wavelength of 800 nm at a normalized thickness of $\bar{t}$ = 0.8 is observed in Figure 3a, consistent with previous observations demonstrating the reproducible plasmonics of these substrates. In addition, the SECARS signal obtained for benzenethiol adsorbed on this sample is plotted as a function of film thickness and overlaid on the extinction map. The intensity of the 1070 cm^{-1} Raman scattered peak, corresponding to the ring stretching mode of benzenethiol, is extracted and plotted for each film thickness. Strikingly intense SECARS enhancements are observed when the absorption at the pump, Stokes, and anti-Stokes are strongest, for instance, at $\bar{t}$ = 0.8 for D = 500 nm. Correspondingly, for the D = 800 nm sample we obtain strong SECARS enhancements matching the plasmon extinction over a broad range of thicknesses. The decrease in SECARS intensities between $\bar{t}$ = 0.4 and $\bar{t}$ = 0.55 can be explained by the slight decrease in resonance at the Stokes frequency for those structures. Slices at the three different frequencies for extinction on these samples are provided in the Supporting Information (see Figure S5). The variation in magnitude of enhancements can be attributed to the existence of radiative and nonradiative plasmon modes in these nanostructures that contribute differently to the three separate resonance frequencies.[18,24,26−28] The pump resonance seems to have the largest effect (Supporting Information, Figure S5), which is also consistent with the mechanism of SECARS described later in the paper. However, the observation that high SECARS signals are directly correlated to plasmon resonances is consistent over measurements for other nanovoid substrates with different void sizes (see Supporting Information, Figures S3 and S4). This proves that both the incident lasers and the outgoing radiation need to be in resonance with a plasmon mode for maximum SECARS enhancement. The broad line width of these modes achievable on nanovoids ensures this condition is guaranteed for all involved photons, which is clearly required for maximum SECARS enhancement.

Other four-wave mixing (FWM) processes in addition to CARS are known to occur on metallic surfaces[29,30] and it has also been suggested that FWM processes could be enhanced by surface plasmons.[31−34] However, here we report the CARS that is plasmon-enhanced and depends on the vibrational signature of the molecule. Other FWM processes are indeed also enhanced on our nanostructured surfaces (to be communicated separately). In order to demonstrate that we observe SECARS, we use several Raman active molecules and confirm that the signals are molecule specific. The surfaces are soaked in ethanolic solutions of thiols (benzenethiol, pyridinethiol, nitrilobenzenethiol) or in aqueous solutions of cyanide salts for an hour and then thoroughly washed to ensure no more than monolayer coverage (see Supporting Information, Section 1.3 for details). We utilize polarization-sensitive detection to record the SECARS signal, which suppresses the contributions from other FWM processes.[35] The SECARS spectrum clearly changes with the type of the molecule under study (Figure 4b,c) and although our setup gives a resolution of only >50 cm^{-1} we can still detect differences in the fingerprint region for different molecules with SECARS. The broad peaks in the SECARS spectrum are a result of a

dx.doi.org/10.1021/nl202875w |*Nano Lett.* XXXX, XXX, 000–000

combination of factors, the most important being that the spectra are acquired with a 150 fs pulsed laser with an 8 nm spectral width. Molecules with cyano-groups indeed show their typical peak vibrations at 2100 cm^{-1} demonstrating that the SECARS spectra are molecule specific and that chemically selective imaging is possible. An electronic FWM background that is plasmon enhanced is clearly visible besides the peak especially in the region 1000−1600 cm^{-1}. We observe that this signal is greatly amplified on our nanostructured surface compared to flat gold. Further, we note that the peak for the cyano-group at 2100 cm^{-1} is slightly shifted in SECARS compared to the solution CARS spectra and suggest this could be due to surface interaction on adsorption, although this needs further investigation. In Figure 4c, the symmetric ring stretch at 1100 cm^{-1} is present for both molecules because both have a benzene ring. The 1600 cm^{-1} peak is stronger in NBT compared to BT because of the nitrilo functional group in the former that makes the C−C bond more polarizable. This extra chemical group is responsible for the observed differences between the spectra of NBT and BT. Furthermore, using our monolayer-modified nanovoid samples we are able to calculate the enhancement factor of SECARS in a method analogous to that used in SERS.[18] Detailed information on how the enhancement factor has been calculated can be found in the Supporting Information (Section 5). We find that SECARS signals in our experiments are enhanced by $\sim 10^5$ over CARS.

Furthermore, by incorporating additional Raman detection functionality within the same setup (using the same pump laser operated in CW mode) we performed SERS measurements on the same nanovoid surfaces discussed above. Using this data we are able to calculate the SECARS enhancements over Stokes SERS, comparing the signal output for a given laser power incident on the sample. We find an additional enhancement of $\sim 10^3$ in SECARS signals over SERS for benzenethiol. Considering the fact that SERS on nanovoid surfaces for benzenethiol is itself enhanced by $\sim 10^6-10^7$ both in the visible and near-infrared,[25,36] the overall enhancement in SECARS is estimated to be $\sim 10^9-10^{10}$ on nanovoid surfaces. These levels of enhancement pave the way for its utilization for ultrasensitive monitoring and single-molecule spectroscopy.[37]

The large enhancements in SECARS arise from the increased plasmonic coupling at the nanovoid surfaces in a process analogous to SERS[18,38] although here there are some prominent differences. In SECARS, the three ingoing photons (two pump, one Stokes) of the two excitation beams both interact with the surface exciting plasmons. All three plasmons act coherently on the molecule forcing it to undergo a CARS transition. We propose the following mechanism: the incident pump photon couples into a plasmon (pump plasmon) that polarizes the molecule adsorbed on the surface (Figure 4a). The Stokes and the pump plasmon then act in tandem forcing the molecule into the first excited vibrational state from where it is pumped into another virtual state. The molecule changes its vibrational state again and its polarization alters. This change is coupled out in a blue-shifted anti-Stokes plasmon. Finally this plasmon couples into an emitted CARS scattered photon.

It is well-known that the intensity of conventional CARS signals results from the third order nonlinear polarization and is dependent on the square of the pump and linearly on the Stokes field intensity[6]

$$I_{CARS} \propto I_p^2 I_S$$

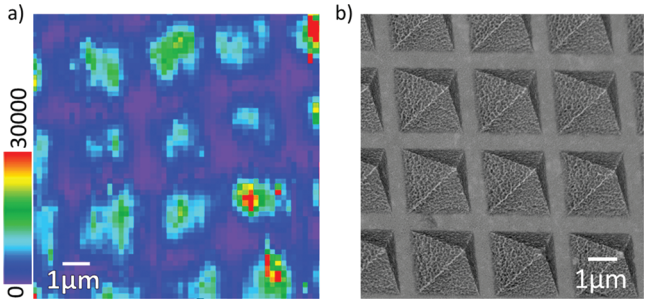

Figure 5. (a) SECARS image of benzenethiol monolayer on the commercially available plasmonic surface Klarite. The color of each pixel tracks the peak intensity at 1070 cm^{-1} extracted from each SECARS spectrum taken with integration time of 10 ms every 300 nm using a 100× objective. (b) Scanning electron microscopy image of the same area showing the pyramidal pits of Klarite.

We investigated the power dependence of SECARS signals on nanovoid surfaces with respect to both the pump and Stokes beams. This is verified to have the correct dependence, which is quadratic in the pump and linear with the Stokes power (see Supporting Information, Figure S6). However, in SECARS, the enhanced intensity must take into account all four involved plasmons including the outgoing anti-Stokes, which leads to an overall enhancement factor G given by

$$G_{SECARS} = g_P^4 g_S^2 g_{aS}^2$$

where $g = E/E_0$ is the enhancement in local optical field at that frequency. It is this eighth power dependence which results in high enhancements in SECARS over CARS. Moreover, there is an additional enhancement factor in SECARS over SERS given by

$$\frac{G_{SECARS}}{G_{SERS}} = g_P^2 g_{aS}^2$$

To demonstrate the molecular imaging abilities of SECARS we used the commercially available plasmonic substrate Klarite. This is based on a different (pyramidal) void architecture and is uniformly reproducible over large areas[39] though of slightly weaker enhancement. An SEM image of a Klarite surface consisting of micro pyramid pits with a lattice pitch of 2.5 μm is shown in Figure 5. Klarite supports strongly localized plasmons and has been successfully applied to SERS.[40,41] Due to the adiabatic taper into the pits, their plasmon absorption is also very broad, with strong absorption from 600 nm to 900 nm (see Supporting Information, Figure S8), which makes them an ideal substrate for SECARS.

Similar to nanovoid surfaces, the Klarite substrate was also coated with a benzenethiol monolayer. An XY stage with a 230 nm step size was used to scan the sample and a SECARS spectrum was recorded on each spot. Because of the massive enhancement of SECARS, an integration time of less than 10 ms is sufficient to record spectra with large signal-to-noise ratios. It is worth noting that SECARS signals were stable over 10 000 such measurements at each point (see Supporting Information, Figure S7), demonstrating the lack of bleaching or instability from the weak laser beams utilized which is crucial for real imaging applications. A SECARS map consisting of 2500 full spectra (50 × 50) pixels takes less than 25 s; much faster imaging can be easily achieved with detection schemes based on single photon counting. Compared to SERS mapping of a similar monolayer, this scanning

dx.doi.org/10.1021/nl202875w |Nano Lett. XXXX, XXX, 000–000

speed is a dramatic improvement. Extracting peak intensities at 1070 cm^{-1} allows the image in Figure 5a to be reconstructed, clearly showing strong peak enhancements inside the pyramidal pit where the most strong intensities caused by the local field enhancements occur.[40] Since plasmons are not well supported in between the pits on Klarite substrates, these positions show only weak signals due to a lack of enhancement. This further demonstrates that plasmon coupling is crucial to large SECARS enhancements. SECARS on reproducible plasmonic surfaces is ideal for their utilization in molecular imaging of biomolecules and cellular membrane immobilized structures. The ability to watch trafficking of proteins through cell-membranes in real-time, for instance, is enabled by use of SECARS which can potentially reach single-molecule sensitivity without using high laser powers that lead to molecular damage.

In conclusion, we demonstrate strong surface-enhanced CARS from plasmonic nanostructures. We have clearly shown the plasmonic dependence and molecular specificity of SECARS. We have also studied the enhancement factors and have proposed a plasmon-aided mechanism of SECARS. Enhancement factors exceeding 5 orders of magnitude over CARS could be observed. SECARS has been shown to have higher sensitivity than SERS with overall enhancements of $\sim 10^9 - 10^{10}$ over conventional Raman spectroscopy. We have also demonstrated rapid imaging of monolayers with SECARS. Our work paves the way for reliable single molecule spectroscopy and fast yet sensitive molecular imaging with SECARS.

■ ASSOCIATED CONTENT

Supporting Information. Details of the broadband CARS setup, absorption maps and SECARS measurements on different nanovoid surfaces, extinction slices at different frequencies, power dependence of SECAR signals, stability data of SECARS, absorption map of Klarite, and details on calculation of enhancement factors is available. This material is available free of charge via the Internet at http://pubs.acs.org.

■ AUTHOR INFORMATION

Corresponding Author

*E-mail: (S.M.) sm735@cam.ac.uk; (J.J.B.) jjb12@cam.ac.uk.

■ ACKNOWLEDGMENT

We gratefully acknowledge support from U.K. EPSRC Grants EP/F059396/1, EP/G060649/1, EP/F028261/1 and Renishaw Diagnostics Ltd. S.M. would like to thank the EPSRC for a fellowship (EP/H028757/1). We thank Physik Instrumente GMBH, Karlsruhe for providing us with a P-545.3R7 piezo stage for performing the imaging experiments above.

■ REFERENCES

(1) McReery, R. *Raman Spectroscopy for Chemical Analysis*; John Wiley & Sons: New York, 2000.
(2) Minck, R. W.; Terhune, R. W.; Rado, W. G. *Appl. Phys. Lett.* **1963**, *3*, 181–184.
(3) Zumbusch, A.; Holtom, G. R.; Xie, X. S. *Phys. Rev. Lett.* **1999**, *82*, 4142–4145.
(4) Fleischmann, M.; Hendra, P.; McQuillan, A. *Chem. Phys. Lett.* **1974**, *26*, 163–166.
(5) Jeanmaire, D. L.; Van Duyne, R. P. *J. Electroanal. Chem.* **1977**, *84*, 1–20.
(6) Kneipp, K.; Moskovits, M.; Kneipp, H. *Surface-enhanced raman scattering: physics and applications*. Springer: New York, 2006.
(7) Lakowicz, J. R. *Anal. Biochem.* **2001**, *298*, 1–24.
(8) Koo, T.; Chan, S. *Opt. Lett.* **2005**, *30*, 1024–1026.
(9) Liang, E.; Weippert, A.; Funk, J. M.; Materny, A.; Kiefer, W. *Chem. Phys. Lett.* **1994**, *227*, 115–120.
(10) Namboodiri, V.; Namboodiri, M.; Diaz, G. I. C.; Oppermann, M.; Flachenecker, G.; Materny, A. *Vib. Spectrosc.* **2010**, 8–11.
(11) Addison, C. J.; Konorov, S. O.; Brolo, A. G.; Blades, M. W.; Turner, R. F. B. *J. Phys. Chem. C* **2009**, *113*, 3586–3592.
(12) Ichimura, T.; Hayazawa, N.; Hashimoto, M.; Inouye, Y.; Kawata, S. *J. Raman Spectrosc.* **2003**, *34*, 651–654.
(13) Hayazawa, N. *Jpn. J. Appl Phys.* **2004**, *95*, 2676.
(14) Ichimura, T.; Hayazawa, N.; Hashimoto, M.; Inouye, Y.; Kawata, S. *Phys. Rev. Lett.* **2004**, *92*, 20–23.
(15) Chew, H. *J. Opt. Soc. Am. B* **1984**, *6*, 4370.
(16) Blaber, M. G.; Schatz, G. C. *Chem. Commun.* **2011**, *47*, 3769–71.
(17) Mahajan, S.; Baumberg, J. J.; Russell, A. E.; Bartlett, P. N. *Phys. Chem. Chem. Phys.* **2007**, *9*, 6016–20.
(18) Baumberg, J. J.; Kelf, T. A.; Sugawara, Y.; Cintra, S.; Abdelsalam, M. E.; Bartlett, P. N.; Russell, A. E. *Nano Lett.* **2005**, *5*, 2262–7.
(19) Kelf, T.; Sugawara, Y.; Cole, R.; Baumberg, J.; Abdelsalam, M.; Cintra, S.; Mahajan, S.; Russell, A.; Bartlett, P. *Phys. Rev. B* **2006**, *74*, 1–12.
(20) Mahajan, S.; Cole, R. M.; Soares, B. F.; Pelfrey, S. H.; Russell, A. E.; Baumberg, J. J.; Bartlett, P. N. *J. Phys. Chem. C* **2009**, *113*, 9284–9289.
(21) Perney, N.; García de Abajo, F.; Baumberg, J.; Tang, A.; Netti, M.; Charlton, M.; Zoorob, M. *Phys. Rev. B* **2007**, *76*, 1–5.
(22) Bartlett, P. N.; Birkin, P. R.; Ghanem, M. A. *Chem. Commun.* **2000**, 1671–1672.
(23) Cole, R. M.; Baumberg, J. J.; Garcia de Abajo, F. J.; Mahajan, S.; Abdelsalam, M.; Bartlett, P. N. *Nano Lett.* **2007**, *7*, 2094–2100.
(24) Mahajan, S.; Cole, R. M.; Soares, B. F.; Pelfrey, S. H.; Russell, A. E.; Baumberg, J. J.; Bartlett, P. N. *J. Phys. Chem. C* **2009**, *113*, 9284–9289.
(25) Mahajan, S.; Abdelsalam, M.; Suguwara, Y.; Cintra, S.; Russell, A.; Baumberg, J.; Bartlett, P. *Phys. Chem. Chem. Phys.* **2007**, *9*, 104–9.
(26) Kelf, T.; Sugawara, Y.; Cole, R.; Baumberg, J.; Abdelsalam, M.; Cintra, S.; Mahajan, S.; Russell, A.; Bartlett, P. *Phys. Rev. B* **2006**, *74*, 1–12.
(27) Cole, R. M.; Mahajan, S.; Bartlett, P. N.; Baumberg, J. J. *Opt. Express* **2009**, *17*, 13298–308.
(28) Le Ru, E. C.; Galloway, C.; Etchegoin, P. G. *Phys. Chem. Chem. Phys.* **2006**, *8*, 3083–7.
(29) Danckwerts, M.; Novotny, L. *Phys. Rev. Lett.* **2007**, *98*, 1–4.
(30) Wang, Y.; Lin, C.-Y.; Nikolaenko, A.; Raghunathan, V.; Potma, E. O. *Adv. Opt. Photonics* **2010**, *3*, 1.
(31) Palomba, S.; Danckwerts, M.; Novotny, L. *J. Opt. A: Pure Appl. Opt.* **2009**, *11*, 114030.
(32) Palomba, S.; Novotny, L. *Phys. Rev. Lett.* **2008**, *101*, 2–5.
(33) Liu, X.; Wang, Y.; Potma, E. O. *Opt. Lett.* **2011**, *36*, 2348–2350.
(34) Renger, J.; Quidant, R.; van Hulst, N.; Novotny, L. *Phys. Rev. Lett.* **2010**, *104*, 2–5.
(35) Cheng, J.; Book, L. *Opt. Lett.* **2001**, *26*, 1341–1343.
(36) Cintra, S.; Abdelsalam, M. E.; Bartlett, P. N.; Baumberg, J. J.; Kelf, T. A.; Sugawara, Y.; Russell, A. E. *Faraday Discuss.* **2006**, *132*, 191–199.
(37) Blackie, E. J.; Le Ru, E. C.; Etchegoin, P. G. *J. Am. Chem. Soc.* **2009**, *131*, 14466–72.
(38) Baltog, I.; Primeau, N.; Reinisch, R.; Coutaz, J. L. *Appl. Phys. Lett.* **1995**, *66*, 1187.
(39) http://www.renishawdiagnostics.com. (accessed August 1, 2011).
(40) Perney, N. M. B.; Baumberg, J. J.; Zoorob, M. E.; Charlton, M. D. B.; Mahnkopf, S.; Netti, C. M. *Opt. Express* **2006**, *14*, 847–57.
(41) Perney, N.; García de Abajo, F.; Baumberg, J.; Tang, A.; Netti, M.; Charlton, M.; Zoorob, M. *Phys. Rev. B* **2007**, *76*, 1–5.